Characterization of Ionic Liquid Multimode Propellant Operating in a Porous Glass Electrospray Thruster

IEPC-2022-500

Presented at the 37th International Electric Propulsion Conference
Massachusetts Institute of Technology, Cambridge, MA, USA
June 19-23, 2022

Anthony C. Adduci[1], Joshua L. Rovey[2], Chrstopher T. Lyne[3], Zachary R. Putnam[4], and Michael F. Lembeck[5]
University of Illinois Urbana-Champaign, Urbana, IL, 61801

Chengyu Ma[6] and Charles N. Ryan[7]
University of Southampton, Southampton, Hampshire, United Kingdom, SO17 1BJ

Steven Berg[8]
Froberg Aerospace LLC., Wilmington, NC 28401, United States

Multimode space propulsion is an emerging technology that shows a promising increase in mission flexibility, adaptability, and mass savings for specific missions [1]. Finding a propellant that operates well in multiple propulsive modes is a key step in getting multimode propulsion systems flying in space. This study characterizes a novel multimode propellant named FAM-110A through operation in a porous glass electrospray thruster. Measurements acquired include current-voltage characteristic curves, plume energy via a retarding potential analyzer, and mass to charge ratio via a linear time of flight spectrometer. It is demonstrated that FAM-110A operates stably in cation emission, anion emission, and bipolar operational modes. The propellant has a higher onset voltage and emits less current than EMIM BF_4 operating in the same thruster. The electrospray plume emitted during operation with FAM-110A appears to be monoenergetic and the time of flight data indicates that the EMIM monomer species is most likely the dominant species being emitted during cation emission operation.

I. Nomenclature

q = ion charge
m = ion mass
L_0 = ToF spectrometer fligh tube length
t_f = particle flight time
V_B = electropsray plume potential

[1]Graduate Research Assistant, Department of Aerospace Engineering, University of Illinois Urbana-Champaign, 104 S. Wright St. Urbana,IL United States
[2]Associate Professor, Department of Aerospace Engineering, University of Illinois Urbana-Champaign, 104 S. Wright St. Urbana,IL United States
[3]PhD Candidate, Department of Aerospace Engineering,University of Illinois Urbana Champaign, 104 S. Wright St. Urbana,IL United States
[4]Assistant Professor, Department of Aerospace Engineering, University of Illinois Urbana-Champaign,104 S. Wright St. Urbana,IL United States
[5]Clinical Associate Professor, Department of Aerospace Engineering, 104 S. Wright St. Urbana,IL United States
[6]Research Fellow, Department of Aeronuatics and Astronautics, University of Southampton, Southampton, Hampshire, SO17 1BJ, United Kingdom
[7]Lecturer/Assistant Professor, Department of Aeronuatics and Astronautics, University of Southampton, Southampton, Hampshire, SO17 1BJ, United Kingdom
[8]Chief Executive Office, Froberg Aerospace LLC, 226 N. Front St. Ste. 123, Wilmington, NC 28401, United States

II. Introduction

Multimode in-space propulsion consists of integrating two or more propulsive modes into a single system with a shared propellant. The sharing of propellant between propulsive modes introduces increased mass savings, enablement of new missions, and in situ mission adaptability [1]. Multimode propulsion systems typically integrate a high thrust chemical mode and a low thrust, high specific impulse electric mode to encapsulate a large mission space [2]. One promising chemical-electric multimode sytem being developed by the Electric Propulsion Laboratory at the University of Illinois Urbana-Champaign consists of a high specific impulse electrospray thruster, and a high thrust chemical monopropellant thruster. The main challenge in the development of a chemical-electric multimode propulsion system is finding a propellant that is suitable for both propulsive modes. A novel green ionic liquid propellant named FAM-110A has been developed by Froberg Aerospace LLC to address the the primary needs of a chemical-electric multimode system. FAM-110A consists of 59% Hydroxylammonium Nitrate (HAN), and 41% Ethyl-3-methylimidazolium ethyl-sulfate (EMIM-EtSO4) by mass [3]. The chemical decomposition of FAM-110A has been demonstrated by Rovey and Berg in a platinum microtube [4], and by Sharma et al. in a platinum catalyst microthruster [5]. In addition to chemical operation, stable electrospray operation of FAM-110A was demonstrated by Rovey and Berg [6], Wainwright et al. [7],[8], and Lyne et al. [3] in a capillary emitter configuration. The performance of this propellant in both modes is important for its success in a multimode space propulsion system.

An electrospray thruster operates by extracting and accelerating charged particles (ions or droplets) with electrostatic fields. Charged particles are extracted from an ionic liquid by applying an electric field between the emitter tip and extractor electrode. The imbalance between the surface tension of the liquid and the electrostatic force gives rise to the emission of the charged particles. In a porous emitter configuration (the configuration of interest in this paper), a porous material is etched into a conical structure. Liquid wicks through the pores of the material towards the sharp tip and charged particles are then emitted from the pours when an electric field is applied. Porous emitter configurations are particulary advantages as they enable simple capillary driven, zero gravity compatible passive feeding of propellant [9]. This could reduce the mass, power, and volume requirements of a thruster by eliminating feed system components. A porous glass thruster can also operate in a bipolar mode, switching the polarity of the emitter voltage, enabling operation without the use of an external neutralizer.

Stable operation of a porous glass electrospray thruster has been demonstrated by Ma and Ryan [10] in the PET-100 thruster developed at University of Southampton. The PET-100 and other works investigating porous electrospray thrusters [9], demonstrate highly ionic emission. Ma and Ryan also did a mission performance evaluation of the PET-100 thruster [11] demonstrating relatively high specific impulse, ranging from 3500 to 7500 seconds and a wide range of thrust from sub-μN to more than 260 μN. Natisin et al. developed a fully conventially machined, high performance porous glass electrospray thruster and characterized its performance operating with 1-Ethyl-3-methylimidazolium tetrafluoroborate (EMIM BF_4) [12]. The thruster operated successfully at emission currents up to $\pm$700 μA at applied emitter voltages of +1845 V and -1835 V for cation and anion emission, respectively. The fraction of the total current intercepted by the extractor grid was below 1% at emission currents up to 500 μA in positive mode and -700 μA in negative mode.

This paper investigates the electrospray performance and plume characteristics of the FAM-110A propellant through operation in a porous glass electrospray thruster manufactured at University of Illinois Urbana-Champaign. Current-voltage charactertistic curves are measured for both FAM-110A and EMIM-BF_4. A retarding potential analyzer is used to measure the energy of the beam, and time of flight spectrometry is used to determine the plume composition of FAM-110A propellant. This characterization will assess the propellants viability as a candidate for use in a multimode space propulsion system that consists of a chemical monopropellant thruster and porous glass electrospray thruster. The remainder of this paper is laid out as follows: an overview of the thruster design and fabrication, the experimental set up and a summary of the diagnostics used, results from thruster testing, discussion of the results, and conclusions drawn from this test campaign.

III. Thruster Overview

A. Thruster Design and Fabrication

The thruster described here was fabricated and tested in the Electric Propulsion Laboratory at the University of Illinois Urbana-Champaign. The thruster design is based on the Air Force Electrospray Thruster Series 2 (AFET-2) [12], which was proposed as a high performance conventionally machined porous-media electrospray thruster to enable

more wide spread research on this technology. An exploded view and an example of the fully assembled thruster is found in Fig. 1. The thruster consists of an aluminum housing, an emitter housing machined from PEEK, a spring, a porous borosilicate glass reservoir, a filter paper interface, a porous borosilicate glass emitter array, a stainless steel distal electrode, a high voltage connection, and a stainless steel extractor grid. There are four set screws at the bottom of the housing that move vertically to adjust the emitter height. There are eight set screws, two at each corner, around the perimeter of the extractor grid for x and y plane translation. The emitter array consists of 576 emitters machined from P5 grade porous borosilicate glass. The design proposed by Natisin et al. [12] calls for machining the emitter structures to a height of 300 μm using a CNC machine with a spindle speed of 50,000 RPM. The thruster manufactured at the University of Illinois was machined using a spindle speed of only 5,000 RPM. This limitation has led to the emitter array showing some non-uniformity between the emitter heights. To quantify this, the emitter array was imaged using a 3D laser scanning confocal microscope. From the microscope data, the emitter heights can be measured and the overall shape of the structures can be analyzed. It was found that the emitters have a mean height of 172 μm with a standard deviation of 45 μm. The mean radius of curvature of the emitter tips was approximately 33.4 μm. A 3D laser image of the emitter structures can be found in Fig. 2.

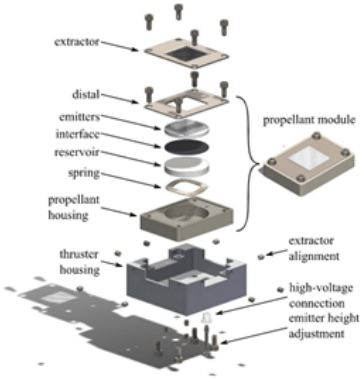

(a) Exploded View of Thruster from [12]

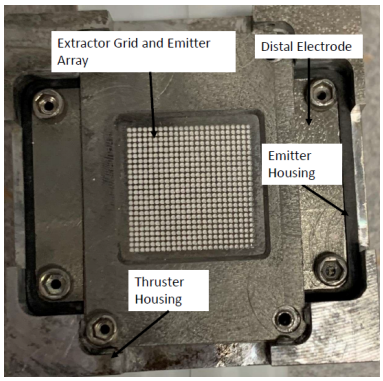

(b) Assembled Thruster

Fig. 1 Porous Glass Electrospray Thruster

The extractor grid is a two piece design consisting of a thin extractor grid, and a thicker extractor frame that are bonded together. The extractor grid component was machined from a 76 μm thick stainless steel sheet using conventional CNC milling. Stainless steel was chosen over molybdenum due to the RPM limitation of the machines at the University of Illinois Urbana-Champaign. The extractor frame component was machined from a 76 μm thick stainless steel plate. The two components were then bonded together using a two part silver conductive epoxy. The extractor grid holes have an aperture diameter of 508 μm and a pitch of 546 μm.

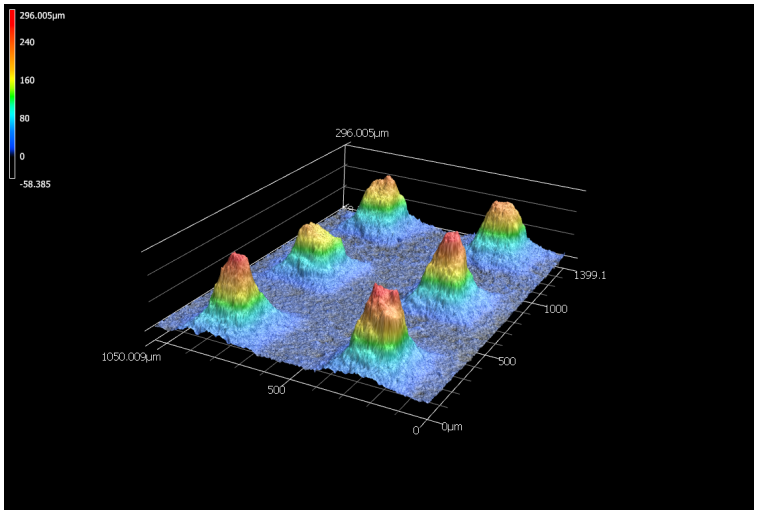

Fig. 2 3D confocal image of emitter structures.

B. Thruster Alignment and Loading Procedure

The emitter-extractor grid alignment and propellant loading procedure described by Natisin et al. [12] is as follows: fully assemble the thruster, align the tips of the emitter structures with the center of the extractor grid holes under an optical microscope using the eight set screws around the perimeter of the extractor grid, use the four set screws at the base of the aluminum housing to raise the emitter array until the tips of the structures are in the same plane as the base of the extractor grid, remove the extractor grid, drip propellant directly onto the emitter array, place the extractor grid back onto the thruster, check the alignment and make any necessary adjustments.

With the thruster manufactured at the University of Illinois, it was found that in order to remove the extractor grid after alignment, the set screws had to be backed out. Once propellant was loaded directly onto the emitter array, the extractor grid would then have to be realigned with the emitter tips. When propellant saturates the porous emitter array, the borosilicate glass changes from white to transparent. The alignment procedure using an optical microscope is then unsatisfactory to achieve good emitter-extractor alignment. To ensure good alignment post propellant loading, the thruster was altered to allow for propellant loading from the rear, leaving the extractor grid fixed. A 0.25 inch hole was drilled in the base of the aluminum housing and PEEK emitter housing exposing the porous propellant reservoir as seen in Fig. 3a. The thruster is then aligned before any propellant is loaded ensuring good alignment is achieved under an optical microscope. The four set screws at the base of the aluminum housing are used to raise the emitters decreasing the gap between the emitter tips and the extractor. At this point, the thruster is imaged using a 3D laser scanning confocal microscope to quantify the alignment and gap distance between the emitter and extractor. Fig. 3b shows a 3D height map of the extractor grid and emitter tips. The distance between each emitter tip and the bottom plane of each extractor hole is measured producing a distribution of the gap distance. The radial distance from each emitter tip to the center of each extractor hole is also measured producing a distribution that represents the alignment quality of each test. A perfect alignment of one emitter to tip to its respective extractor grid hole would yield a radial distance of 0 μm. The thruster is then positioned extractor grid side down on a ring stand. Propellant is dripped directly onto the exposed porous reservoir using a syringe and left to flow down through the reservoir and into the emitter array. A multimeter is used to measure the resistance between the porous reservoir and the distal electrode. Prior to propellant loading, the resistance measurement is out of range of the multimeter (> 60MΩ). It was found that when the emitter array is fully saturated, the resistance is approximately 12 MΩ. At this point, the thruster is fully loaded with propellant, aligned, and ready for testing.

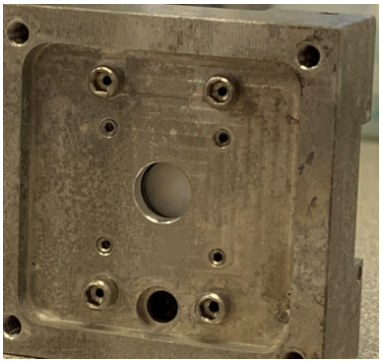

(a)

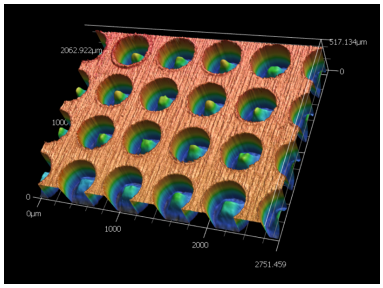

(b)

Fig. 3 Image of (a) the propellant inlet hole in the rear of the thruster and (b) a 3D confocal scan of the assembled thruster for gap distance and alignment quantification.

IV. Experimental Set Up

This test campaign was carried out in a vacuum chamber pumped using a mechanical roughing pump and a turbo pump. Chamber pressure was approximately 10^{-6} Torr at the beginning of thruster operation. The thruster was passively fed propellant for all tests; the propellant was loaded directly onto the porous glass reservoir and emitter array, so an external feed system was not needed. The diagnostics used for plume characterization consisted of a 316 stainless steel collector plate, a retarding potential analyzer, and a linear time of flight spectrometer. The thruster was positioned on a vacuum compatible rotary stage allowing for rapid transition from one diagnostic technique to another. Fig. 4 shows a schematic of the experimental set up, as well as an image of the thruster positioned inside of the chamber aligned along the centerline of the collector plate. The thruster was operated with 1-Ethyl-3-methylimidazolium tetrafluoroborate (EMIM BF_4), a widely used electrospray propellant, and FAM-110A for comparison of the measured plume characteristics.

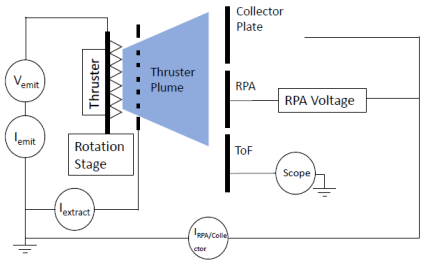

(a)

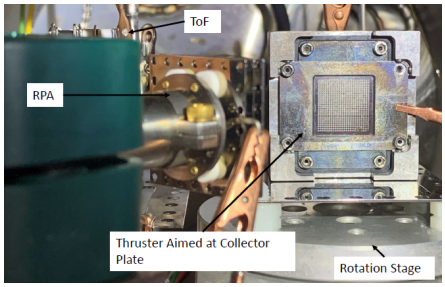

(b)

Fig. 4 Image of (a) the experimental set up diagram (b) the thruster mounted to the rotation stage inside of the vacuum chamber.

A. Emitter, Extractor, and Collector Current

A 316 stainless steel collector plate was used to intercept the thruster plume and measure the current as a function of the applied emitter voltage during operation. The plate was built to catch the plume up to 45° off centerline. Measurements were made with the same instrumentation set up used by Lyne et al. [3] to characterize FAM-110A electrospray performance through operation in a capillary style thruster. Emitter current was measured using a current shunt and high voltage isolation amplifier (Texas Instruments AMC1311) to interface with a National Instruments data acquisition (DAQ) module (NI USB-6210). Extractor current was measured using a standard transimpedance amplifier configuration and recorded using the DAQ. Collector current was measured using a picoammeter (Keithley Model 6485)

and recorded by the DAQ.

B. Retarding Potential Analyzer

A retarding potential analyzer was used to measure the kinetic energy profile of the electropsray plume, as is commonly done in the characterization of ion sources. RPA data were collected using a single grid RPA and a Faraday cup. The current collected by the Faraday cup was recorded as the retarding grid voltage was swept between ground and ±3500 V, keeping the polarity matching the emitter bias polarity. The current was then differentiated with respect to the retarding grid bias to yield the intensity v.s. retarding grid bias, representing the energy profile of the electrospray plume.

C. Time of Flight Spectrometer

A linear time of flight spectrometer was used to measure the mass to charge ratio of emitted particles to identify the species in the beam. Time of flight spectrometry measures the time taken for a charged particle to traverse a certain distance in a region free of external fields, thus allowing the particle velocity to be calculated. If the velocity is gained by acceleration through a known potential, then the mass to charge ratio can be computed [13]. This is shown in equation 1 below.

$$\frac{q}{m} = \frac{(L_0/t_f)^2}{2V_B} \tag{1}$$

Where L_0 is the field free flight tube length, t_f is the time of flight as measured by the instrument, and V_B is the potential of the plume as measured by the retarding potential analyzer. The linear time of flight used in this test campaign featured a flight tube length of 116 mm. The thruster was positioned on centerline of the flight tube and the emitter was biased to +2.9 kV. The gate was biased at some voltage above the emitter voltage to block any charged particles from entering the flight tube initially; once triggered, the gate opened and the time taken for charged particles to traverse the field free flight tube was measured. A more detailed description and study of the time of flight operation is presented in [14].

V. Results

A. EMIM-BF_4

The porous glass electropspray thruster was operated with the commonly used electrospray propellant, EMIM-BF_4. Current-voltage characteristic curves were measured during bipolar operation by sweeping the emitter bias between approximately ±1 kV and ± 1.98 kV. The mean emitter-extractor gap was 128 μm reaching a minimum value of 2.5 μm and a maximum value of 268 μm. The collector plate and extractor current were measured as function of the applied emitter voltage during thruster operation and are shown in Fig. 5 and 6, respectively. The onset voltage was approximately 1483 V. The thruster emitted a higher cation current than anion current with a maximum measured cation current of 134 μA at an operating voltage of 1984 V. The maximum anion current measured was -66 μA at an emitter voltage of 1966 V.

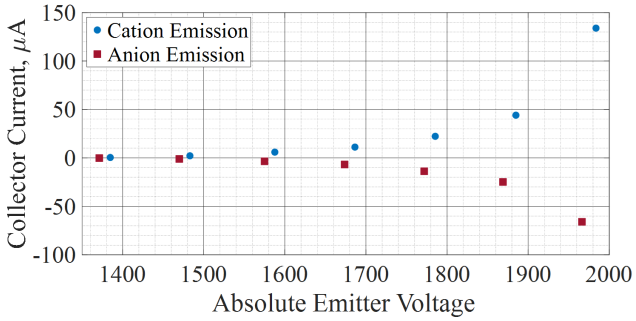

Fig. 5 Collector Current V.S. Applied Emitter Voltage for EMIM-BF_4 During Bipolar Operation

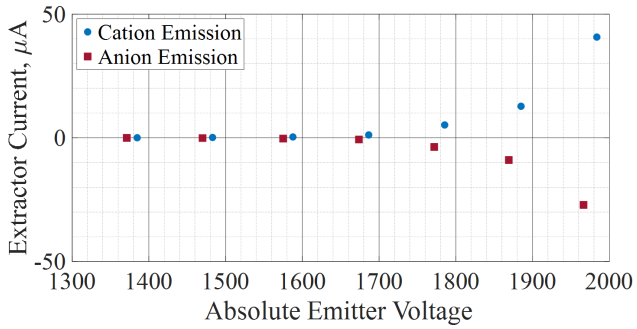

Fig. 6 Extractor Current V.S. Applied Emitter Voltage for EMIM-BF_4 During Bipolar Operation

The trend of the collected current as function of emitter voltage is consistent with the data collected by Natisin et al. [12]; as the magnitude of the emitter voltage increases beyond the onset voltage of the thruster, the collected current increases exponentially. The thruster manufactured at the University of Illinois showed a higher onset voltage and lower collected current at each emitter voltage than the AFET-2 thruster operating with EMIM BF_4. This is a consequence of two factors. First, the emitter array was fabricated at a CNC spindle speed a factor of 10 lower than the speed at which the AFET-2 was fabricated. This has led to non uniformity among the emitter shapes and heights, with the mean height of the emitters being 128 μm less than the height at which the AFET-2 emitters were machined to. Ma [11] studied the effect of a porous emitter's aspect ratio (the emitter's length divided by it's height) on the electric field strength for a single emitter. It was found that when the emitter aspect ratio fell below 1, there was a significant reduction in the electric field strength thus giving rise to a higher onset voltage needed to produce appreciable emission. The radius of curvature, measured to be 33.4 μm, also has an effect on the electric field strength. The AFET-2 thruster had a radius of curvature between 10 and 20 μm. The 10 μm increase in the radius from the maximum of the range will lead to a lower electric field strength, increasing the onset voltage and decreasing the emission current. Second, the fraction of the total emission current intercepted by the extractor grid is much higher than that shown in the AFET-2 thruster. Natisin et al. raised the emitter array such that the tips of the emitters were on the same plane as the bottom of the extractor grid keeping the fraction of the total current impinging on the extractor grid below 1%. During this operation, there was still a mean distance of 128 μm between the tips of the emitters and the bottom of the extractor grid with some emitters being 268 μm below. The larger gap not only leads to a weaker electric field strength, but enables more interception of the plume by the extractor. The fraction of the total current impinging on the extractor grid is plotted as a function of the emitter voltage in Fig. 7.

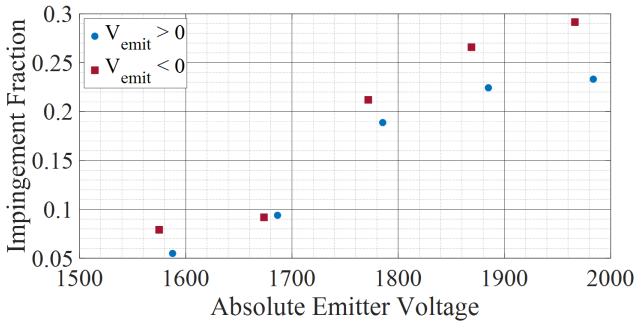

Fig. 7 Beam Current Impingement Fraction as a Function of Emitter Voltage for EMIM-BF_4

The thruster showed a higher impingement fraction with anion emission, reaching a maximum of approximately 29%. The maximum impingement fraction during cation emission was approximately 23%. In both polarities, the impingement fraction increased as a function of the emitter voltage. One possible explanation is the widening of the Taylor cone emission sites as the emitter voltage increases. The wider the emission site, the more current will impinge upon the extractor grid.

B. FAM-110A

A preliminary test of FAM-110A operation in a porous glass electrospray thruster was conducted to demonstrate stable operation. Current-voltage characteristic curves were collected for three operating modes: cation emission, anion emission, and bipolar modes. The thruster emitter was biased while the extractor and collector plate were held at ground potential. For the cation and anion emission modes, the emitter, extractor, and collector currents were measured over an emitter bias range of 1 kV to approximately 3.2 kV in both polarities. In bipolar operation, the current-voltage characteristic was measured by sweeping the emitter bias between ±925 V and ±2800 V. The gap distance between the emitters and the extractor grid was at a maximum for this test with a mean gap distance of 254 μm. The collector current and extractor grid current as a function of the emitter voltage are plotted in Fig. 8 and 9, respectively.

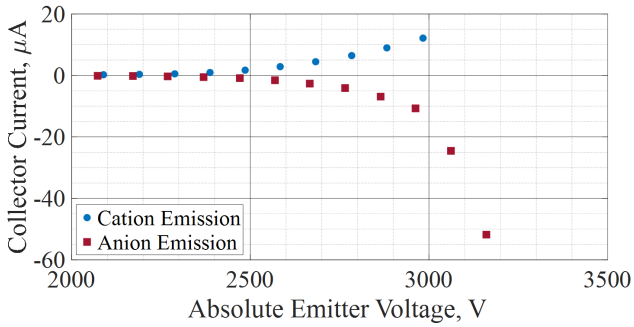

Fig. 8 Collector Current V.S. Emitter Voltage for FAM-110A During Cation and Anion Emission Modes

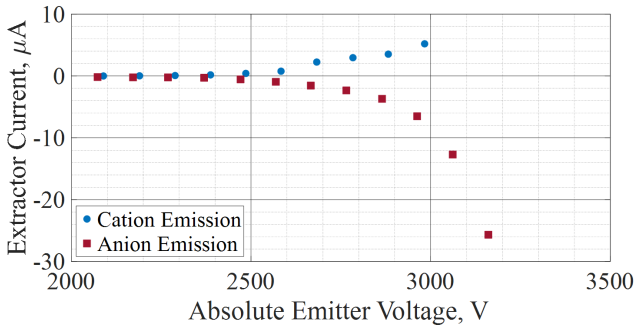

Fig. 9 Collector Current V.S. Emitter Voltage for FAM-110A During Cation and Anion Emission Modes

Fig. 8 shows the thruster had an onset voltage of approximately ±2400 V in both the cation and anion emission modes. The trend of the collector current data is consistent with that produced by the AFET-2 Thruster, as well as the data produced by the University of Illinois thruster operating with EMIM BF_4; as the emitter voltage increases beyond the onset voltage, the collected current increases exponentially. The maximum collected current during cation emission was approximately 12.13 μA at an emitter voltage of 2983 V. The maximum collected current during anion emission was approximately -51.8 μA at an emitter voltage of -3161 V. At an emitter voltage of -2962 V, the collected current was -10.7 μA in anion emission mode. The thruster was also tested in a bipolar mode with a voltage switching frequency of 1Hz; the collected current and extractor current as a function of the emitter voltage is shown in Fig. 10 and 11, respectively.

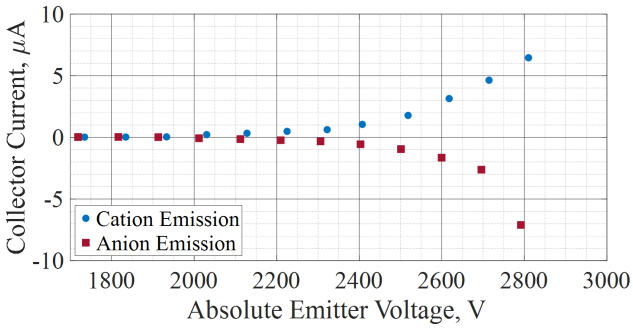

Fig. 10 Collected Current V.S. Emitter Voltage for FAM-110A During Bipolar Operation

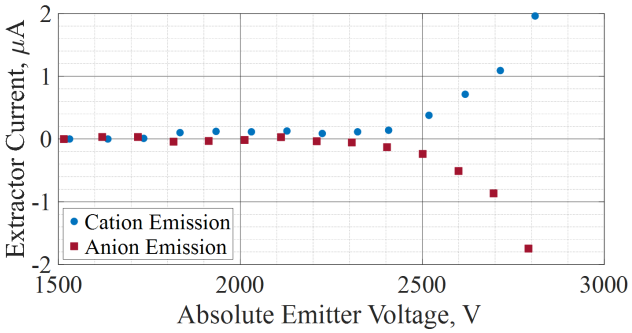

Fig. 11 Extractor Current V.S. Emitter Voltage for FAM-110A During Bipolar Operation

Interestingly, Fig. 10 shows the onset voltage during bipolar operation was approximately 2000 V, a 400 V decrease from what was seen during cation and anion single mode operation. The maximum positive collected current was 6.5 μA at an emitter voltage of +2810 V. The largest negative collected current was -7.1 μA at an emitter voltage of -2792 V. The maximum collected current was approximately 46.4% and 33.6% less than that collected during single mode cation and anion emission, respectively. The fraction of current impinging on the extractor grid was approximately 30% of the total beam current for absolute emitter voltages greater than 2700 V. The high current impingement fraction can be attributed to the large distance between the emitters and extractor grid.

FAM-110A was then tested again in bipolar operation, but the emitter array was raised such that the mean gap distance between the emitter and extractor was approximately 180 μm. The voltage switching frequency was 0.5 Hz. The current data was collected by sweeping the emitter bias between ±0 V and approximately ±3060 V. Fig. 12 below shows the collector plate current as a function of the emitter voltage.

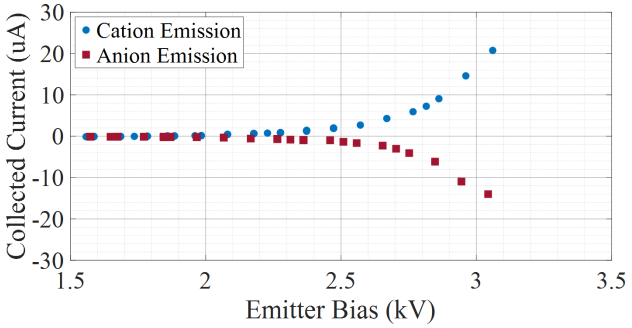

Fig. 12 Collected Current V.S. Emitter Voltage for FAM-110A During Bipolar Operation

In comparison with Fig. 10, the onset voltage was similarly around 2 kV. The maximum cation current measured

was 20.8 μA at an emitter voltage of 3060 V. The maximum anion current measured was -14 μA at an emitter voltage of approximately -3040 V. At an emitter voltage of 2810 V, the collected current was 7.25 μA, an 11.5% increase in cation current collected relative to that shown in Fig. 10. The collected anion current at an emitter voltage of -2792 V was -4.95 μA, a 30.3% reduction in magnitude in comparison to the current measured in Fig. 10. The fraction of the plume current impinging on the extractor reduced as a function of the reduced gap distance comprising of approximately 15% of the total current at voltages greater than 2700 V.

The following RPA and Time of Flight measurements were performed directly following the measurement shown in Fig. 12 i.e. the thruster's emitter to extractor gap distance remained at approximately 180 μm.The energy of the electrospray plume was analyzed using a retarding potential analyzer. The thruster emitter was biased at +3000 V for cation emission and -3000 V for anion emission. Current was collected by a faraday cup as the RPA voltage was swept between 0 and 3500 V, with the bias matching that of the emitter. The current could then be differentiated with respect to the RPA voltage to calculate the intensity of the beam. Due to high frequency noise effecting the slope calculation of the current-voltage curve, the data was filtered using a lowpass filter. Fig. 13 and 14 show the collected current and ion intensity as a function of the RPA bias for cation and anion emission modes, respectively.

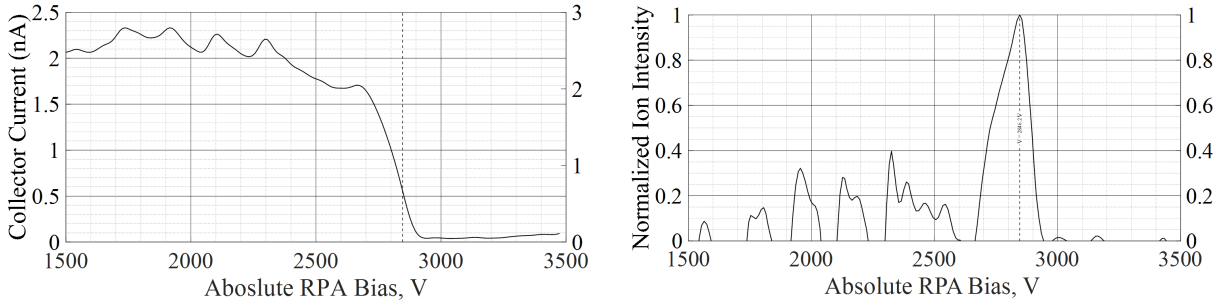

(a) **(b)**

Fig. 13 (a) Current as a Function of RPA Bias and (b) Normalized Ion Intensity as a function of RPA Bias for Cation Emission Mode. Emitter Bias Was Held at +3000 V.

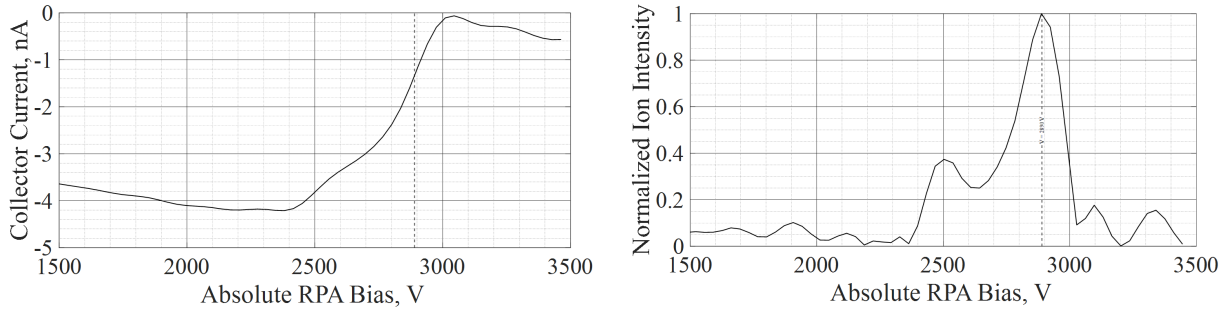

(a) **(b)**

Fig. 14 (a) Current as a Function of RPA Bias and (b) Normalized Ion Intensity as a function of RPA Bias for Anion Emission Mode. Emitter Bias Was Held at -3000 V.

Fig. 13a shows the collected current is relatively constant at approximately 2.2 nA between 0 and 2500 V. The current then decreases as the RPA voltage increases past 2500 Volts. The collected current drops to approximately zero around 2900 Volts. The normalized ion intensity as a function of the RPA voltage, shown in Fig. 13b, shows a distinct peak in this region of current fall off between 2500 and 3000 V reaching a maximum at 2846.2 V. In anion emission mode shown in Fig. 14a, the collected current appears relatively constant at approximately -4.1 nA between 2000 and 2500 volts. As the absolute RPA voltage increases past 2500 V, the magnitude of the current decrease reaching approximately 0 nA at an absolute emitter voltage around 3000 V. The normalized ion intensity as a function of absolute RPA voltage, shown in Fig. 14, shows two different peaks. The peak seen at an absolute RPA voltage of 2500 Volts is

believed to be signal noise due to either the quality of the RPA instrument in use, and/or due to secondary electron emission as a suppression grid was not used. The largest peak seen at 2890 V appears within the region that the faraday cup current decreases and represents the energy of the plume. The data suggests a monoenergetic plume with an energy of 2846.2 V in cation emission mode and 2890 V in anion emission mode.

Fig. 15 gives the flight time data collected by the linear time of flight spectrometer. Only the monomer cation species found in FAM-110A, Hydroxylamine and 1-Ethyl-3-methylimidazolium (EMIM), were considered. The thruster operated in cation emission mode for this test. The data was time shifted to set the time at which the trigger activates and the gate opens to t = 0. The y data has been normalized about the signal at which the charged particles are blocked from entering the flight tube.

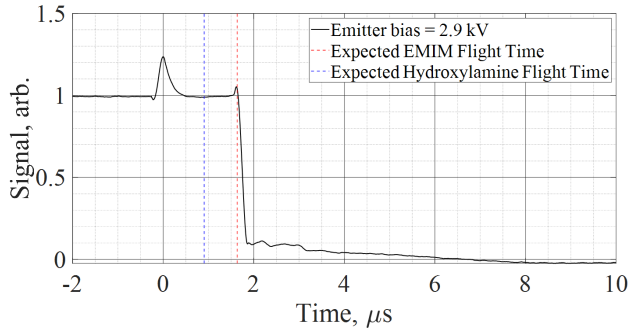

Fig. 15 Measured Flight Times for FAM-110A Plume Species

The data suggests that only a single species was being emitted during thruster operation. At t = 1.75 μs, the entire beam arrives at the detector. The vertical dashed lines represent the expected flight times of hydroxylamine and EMIM monomer species which are 0.9 μs and 1.64 μs repectively. The flight time measured for the FAM-110A plume more closely correlates with that of EMIM, but is approximately 0.11 μs longer. Fig. 16 shows the mass to charge ratio spectrum of the plume computed from the measured flight time data.

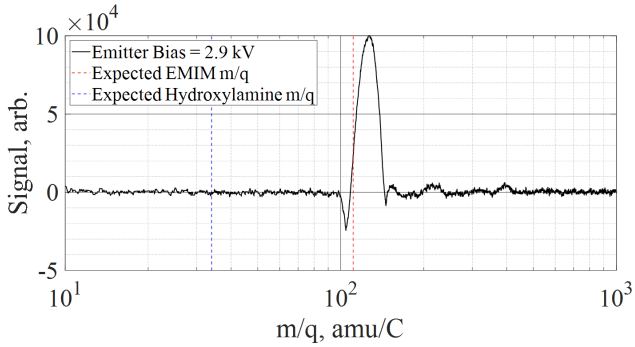

Fig. 16 Mass to Charge Ratio Spectrum for FAM-110A Electrospray Plume

This further suggests a single monomer species present in the plume. The spectrum shows one distinct peak at an m/q value of 126.8 amu/coulomb. The vertical dashed lines represent the m/q ratio of hydroxylamine and EMIM which are 34 and 111 amu/coulomb respectively. The mass to charge ratio is more closely aligned with that of EMIM, but is approximately 15.8 amu/coulomb higher. This discrepancy in mass to charge ratio comes from the 0.11 μs longer flight time measured in the FAM-110A plume than that expected by the EMIM monomer species. A possible explanation for this can be minor uncertainties in the time at which the trigger activates, though the data still strongly suggests a single species plumes consisting of $EMIM^+$ ions.

VI. Conclusions

This paper presents an analysis of the FAM-110A multimode propellant operating in a porous glass electrospray thruster. The thruster design was based on the Air Force Electrospray Thruster Series 2 (AFET-2) [12]. Characterization of the electrospray plume was done through current-voltage characteristic measurements, a retarding potenital analyzer, and a linear time of flight spectrometer. These results show stable operation of FAM-110A in a porous glass electrospray thruster operating in cation emission, anion emission, and bipolar modes. The data collected from the retarding potenital analyzer suggest a monoenergetic plume with minimal losses relative to the emitter bias. The plume energy was measured as 2846.2 V in cation emission mode and 2890 V in anion emission mode. Measurements from the linear time of flight spectrometer suggest single species cation emission when only the monomer species of FAM-110A are considered. The flight time and mass to charge ratio measured more closely align with that of EMIM, suggesting this is the primary monomer species being emitted during cation emission mode. Future work will include improvements in the fabrication techniques of the thruster to produce more uniform emitter and extractor geometries and sharper emitter structure tips. This will improve the overall performance of the thruster and lead to an enhancement in the quality of measurements. A more detailed characterization of EMIM BF_4 will be performed to compare this commonly used electrospray propellant to the data collected for FAM-110A. Finally, the characterization will continue on the FAM-110A multimode propellant and performance metrics such as thrust, mass flow rate, and specific impulse will be computed and analyzed to asses the viability of this propellant to various in space missions.

VII. Acknowledgment

The research reported here was partially supported by the Defense Advanced Research Projects Agency Grant No.: HR00112110003. The content of this paper does not necessarily reflect the position or the policy of the Government, and no official endorsement should be inferred.

References

[1] Rovey, J. L., Lyne, C. T., Mundahl, A. J., Rasmont, N., Glascock, M. S., Wainwright, M. J., and Berg, S. P., "Review of multimode space propulsion," *Progress in Aerospace Sciences*, Vol. 118, 2020. https://doi.org/10.1016/j.paerosci.2020.100627.

[2] Berg, S. P., and Rovey, J. L., "Assessment of Multimode Spacecraft Micropropulsion Systems," 2016. https://doi.org/10.2514/1.A33649, URL www.aiaa.org/randp.

[3] Lyne, C. T., Rovey, J. L., and Berg, S. P., "Monopropellant-Electrospray Multimode Thruster Testing Results: Electrospray Mode," *AIAA Propulsion and Energy Forum, 2021*, 2021. https://doi.org/10.2514/6.2021-3439, URL https://arc.aiaa.org/doi/abs/10.2514/6.2021-3439.

[4] Berg, S. P., and Rovey, J. L., "Decomposition of Double Salt Ionic Liquid Monopropellant in a Microtube for Multi-Mode Micropropulsion Applications," 2017. https://doi.org/10.2514/6.2017-4755, URL http://arc.aiaa.org.

[5] Sharma, A., Adduci, A. C., Rovey, J. L., Putnam, Z. R., Lembeck, M. F., Ryan, C. N., Ma, C., and Berg, S. P., "Green Ionic Liquid Multimode Monopropellant Microthruster," *AIAA Science and Technology Forum and Exposition, AIAA SciTech Forum 2022*, 2022, pp. 1–11. https://doi.org/10.2514/6.2022-1733.

[6] Berg, S. P., Rovey, J. L., Prince, B. D., Miller, S. W., and Bemish, R. J., "Institute for Scientific Research, 140 Commonwealth Ave," *Aberdeen Ave SE. Bldg*, Vol. 570, 2015, p. 3550. https://doi.org/10.2514/6.2015-4011, URL http://arc.aiaa.org.

[7] Wainwright, M. J., Rovey, J. L., Miller, S. W., Prince, B. D., and Berg, S. P., "Electrospray Mass Spectroscopy of a HAN-based Monopropellant," 2018. https://doi.org/10.2514/6.2018-4725, URL http://arc.aiaa.org.

[8] Wainwright, M. J., Rovey, J. L., Miller, S. W., Prince, B. D., and Berg, S. P., "Hydroxylammonium Nitrate Species in a Monopropellant Electrospray Plume," 2019. https://doi.org/10.2514/1.B37471, URL www.aiaa.org/randp.

[9] Courtney, D. G., Dandavino, S., and Shea, H., "Comparing direct and indirect thrust measurements from passively fed ionic electrospray thrusters," *Journal of Propulsion and Power*, Vol. 32, No. 2, 2016, pp. 392–407. https://doi.org/10.2514/1.B35836.

[10] Ma, C., and Ryan, C., "Plume Characterization of a Porous Electrospray Thruster," Tech. rep., 2021.

[11] Ma, C., "Design and Characterisation of Electrospray Thrusters with High Emission Density," Tech. rep., 2020.

[12] Natisin, M. R., Zamora, H. L., McGehee, W. A., Arnold, N. I., Holley, Z. A., Holmes, M. R., and Eckhardt, D., "Fabrication and characterization of a fully conventionally machined, high-performance porous-media electrospray thruster," *Journal of Micromechanics and Microengineering*, Vol. 30, No. 11, 2020, p. 115021. https://doi.org/10.1088/1361-6439/ABB8C3, URL https://iopscience.iop.org/article/10.1088/1361-6439/abb8c3https://iopscience.iop.org/article/10.1088/1361-6439/abb8c3/meta.

[13] Lozano, P., and Martínez-Sánchez, M., "Studies on the Ion-Droplet Mixed Regime in Colloid Thrusters," *Physics*, Vol. 282, No. February, 2003, p. 222. URL http://ssl.mit.edu/publications/theses/PhD-2003-Lozano-TovarPaulo.pdf.

[14] Lyne, C. T., "A low-cost linear time-of-flight mass spectrometer for Electrospray Propulsion Diagnostics," *International Electric Propulsion Conference 2022*, IEPC-2022-178.